Nano Energy 123 (2024) 109398

Contents lists available at ScienceDirect

Nano Energy

journal homepage: www.elsevier.com/locate/nanoen

Full paper

A multi-dimensional tactile perception system based on triboelectric sensors: Towards intelligent sorting without seeing

Tianxiao Xiao [a,1], Zhenshan Bing [b,1], Yansong Wu [b,1], Wei Chen [c,d], Ziming Zhou [d], Fan Fang [d], Suzhe Liang [a], Renjun Guo [a], Suo Tu [a], Guangjiu Pan [a], Tianfu Guan [a], Kai Wang [d], Xiao Wei Sun [d], Kai Huang [e], Alois Knoll [b], Zhong Lin Wang [f,g,*], Peter Müller-Buschbaum [a,h,**]

[a] Chair for Functional Materials, Department of Physics, TUM School of Natural Sciences, Technical University of Munich, James-Franck-Str. 1, Garching 85748, Germany
[b] Chair Robotics, Artificial Intelligence (AI) and Embedded Systems, School of Computation, Information and Technology (CIT), Technical University of Munich, Boltzmannstr. 3, Garching 85748, Germany
[c] College of Engineering Physics, Shenzhen Technology University, Lantian Road 3002, Shenzhen 518118, China
[d] Department of Electrical and Electronic Engineering, Southern University of Science and Technology, Xueyuan Avenue 1088, Shenzhen 518055, China
[e] School of Computer Science, Sun Yat-sen University, 132 Outer Ring East Road, Guangzhou 510006, China
[f] Beijing Institute of Nanoenergy and Nanosystems, Chinese Academy of Sciences, Beijing 101400, China
[g] School of Materials Science and Engineering, Georgia Institute of Technology, Atlanta 30332-0245, USA
[h] Heinz Maier-Leibnitz Zentrum (MLZ), Technical University of Munich, Lichtenbergstr. 1, Garching 85748, Germany

ARTICLE INFO

Keywords:
Triboelectric nanogenerators
Multi-dimensional perception
All-in-one devices
Quantum rods
Intelligent sorting

ABSTRACT

Tactile perception systems as the medium between the ambient environment and robotics lie in the heart of modern artificial intelligence. By providing different electronic readouts under various circumstances, they can give easily captured information for post-processing. However, for applications of most reported tactile perception systems, external location assistances are still needed. Here, as inspired by the platypus' sixth sense, we developed a new kind of tactile perception system based on triboelectric sensors with the additional function from quantum rods. This terminal can be used as a single-electrode mode triboelectric nanogenerator for both location detection and vertical force sensing with high sensitivity and fast response. Moreover, by adding CdSe/CdS quantum rods into an imprinted polydimethylsiloxane film, different lateral stretching levels can be perceived by a modified luminescence. Supported by the machine learning technology, the as-fabricated tactile perception system finally obtains an excellent recognition accuracy among 18 different objects of 98.5% on a micro-controller unit platform, which provides an easy pathway in smart home robotics for intelligent sorting.

1. Introduction

As the largest organ of the human body, skin offers us one of the most important perceptive modes, namely, tactile perception, to sense, interact, extract information, and learn about the surroundings [1,2]. It plays a key role in tasks ranging from object manipulation to social communication. Modeling human skin for tactile perception is becoming one of the hottest research topics in both, material science and robotics [3–14]. Since the birth of skin-like tactile perception systems, a number of devices have been fabricated for various sensing applications via different working mechanisms, such as pressure [15–20], humidity [21,22], temperature [23,24], and magnetic field [25,26]. The current research status in the field of skin-like tactile perception systems is marked by interdisciplinary efforts to improve the durability, sensitivity, and bio-compatibility, which provides tremendous promise for a wide range of applications, including health monitoring, robotics, human-machine interfaces, etc. [14,27]. Today, for most reported tactile perception systems, the signals can only be produced when they are under physical contact conditions. Therefore, external location assistances based on visual images [28], ultrasound transducers [29,30], or

* Corresponding author at: Beijing Institute of Nanoenergy and Nanosystems, Chinese Academy of Sciences, Beijing 101400, China.
** Corresponding author at: Chair for Functional Materials, Department of Physics, TUM School of Natural Sciences, Technical University of Munich, James-Franck-Str. 1, Garching 85748, Germany.
E-mail addresses: zhong.wang@mse.gatech.edu (Z.L. Wang), muellerb@ph.tum.de (P. Müller-Buschbaum).
[1] These authors contributed equally to this work.

https://doi.org/10.1016/j.nanoen.2024.109398
Received 25 December 2023; Received in revised form 29 January 2024; Accepted 14 February 2024
Available online 16 February 2024

electromagnetic technologies [31], are indispensable in their applications. Interestingly, a nocturnal animal in nature named platypus already solved this problem 25 million years ago. During hunting time in the water, a platypus uses its 'duck-billed detector' as the sixth sense instead of eyes, nose and ears to detect the subtle mechanical movements and electric fields produced by its prey (Fig. 1a and b) [32]. Taking the initial inspiration from the platypus' sixth sense, combining location detection and more sensing capabilities into one tactile perception system is highly in demand to mimic better or even surpass human skin.

The newly arising technology called triboelectric nanogenerator (TENG) has emerged since 2012 [33]. TENG is based on the coupling effect of triboelectrification and electrostatic induction, which can directly convert mechanical energy/triggering from the ambient environment into electrical signals [34,35]. In the past decade, owing to the advantages of lightweight, low cost, a diverse choice of materials, and easy fabrication, TENGs as self-powered systems have been widely utilized in giving us a simple solution to obtain the vertical force sensing ability without additional power supplies [6,36–42].

Core/shell quantum rods (QRs) with tunable emission wavelengths and long lifetimes are considered promising materials for light emitters. Recently, many kinds of QRs have been synthesized through different methods for lasing [43,44], photodetector [45], and light-emitting diode (LED) display applications [46,47]. When QRs are under excitation, they can provide condition-dependent visualized light signals. Therefore, adding QRs into a TENG configuration is a promising way to get multi-dimensional sensing capabilities in one tactile perception system.

In this work, we developed a triboelectric sensor based on the single-electrode mode TENG combined with a QRs function added luminescent layer. The non-contact location detection and self-powered vertical force sensing are carried out by the electrical outputs of polydimethylsiloxane (PDMS) based TENG. While the condition-dependent luminescent effect is realized by the functional addition of cadmium selenide/cadmium sulfide (CdSe/CdS) QRs, which can be excited under both, ultraviolet and visible light. Besides, a wavy structure is applied onto the surface of the PDMS composite film for having a higher sensitivity. Additionally, the force-sensing capability remains stable at different stretching levels, demonstrating the independent sensing property of the triboelectric sensor. Finally, the eight triboelectric sensors-based tactile perception system is achieved by the integration of a soft gripper with a computer-controlled robotic arm for intelligent sorting application. Enabled by the electrostatic induction effect of the TENG and our customized data acquisition circuit, the gripper can automatically detect the location of target objects. Then, based on machine learning (ML) technology, the

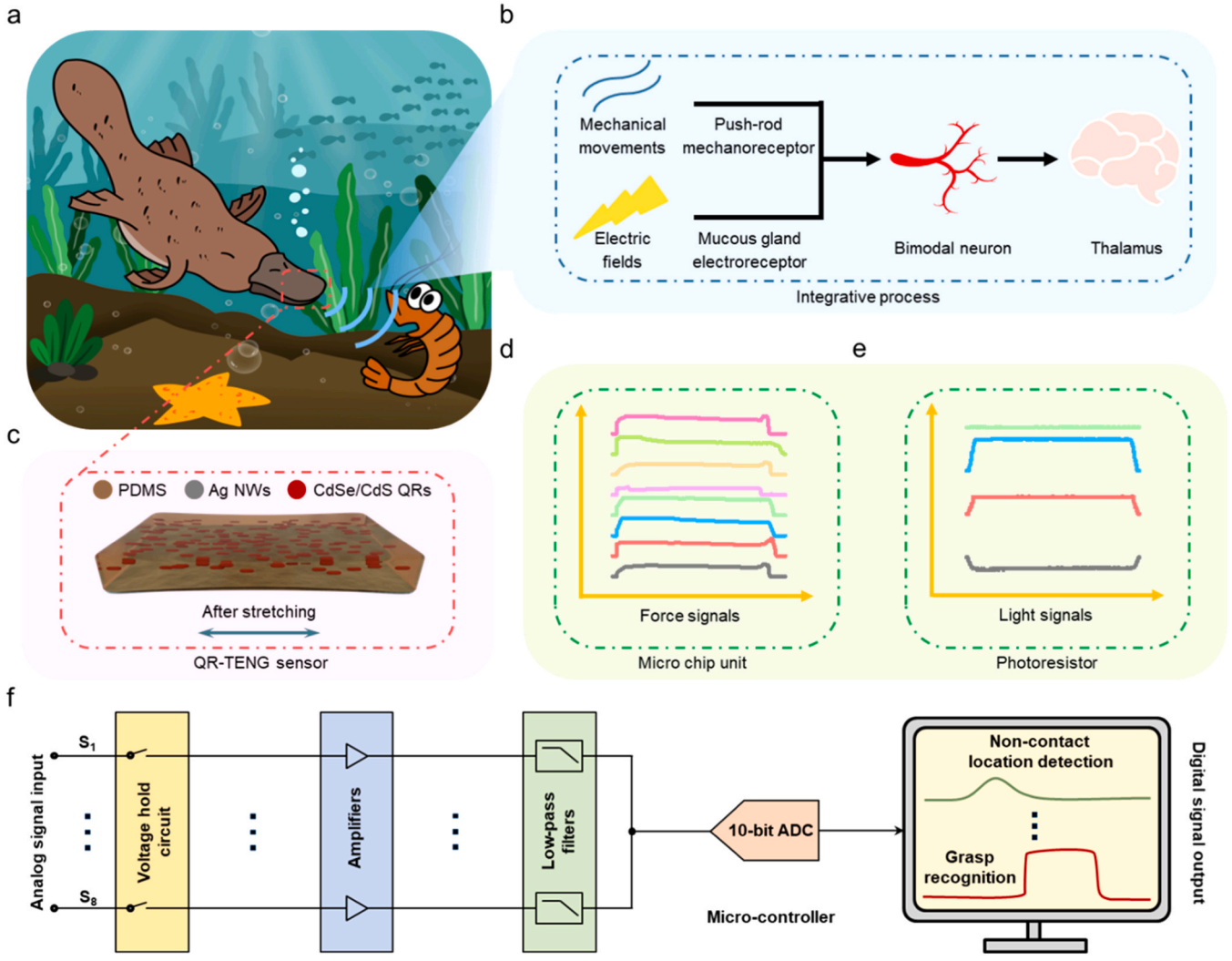

Fig. 1. Quantum rods (QRs) function added triboelectric sensor. (a) Schematic illustration of the platypus using the sixth sense for hunting in the water. (b) Integrative process of the platypus' mechanoreceptive and electroreceptive information. (c) Schematic illustration of the triboelectric sensor with QRs functional addition. (d-e) Typical force and light signals collected by micro-controller unit (MCU) via our custom-made circuit. (f) Circuit diagram showing the signal flow in the real-time perception system, from the collected analog electric signals to the digital signals for the location detection and grasp recognition.

recognition and delivery process is realized by grasp triggers obtained from the triboelectrification effect of the TENG in combination with the luminescent effect of the QRs. As a result, our work realizes a 'without seeing' intelligent sorting through a tactile perception system combining location detection and smart grasp with good robustness and high accuracy on a micro-controller unit (MCU) platform.

2. Experimental section

2.1. Chemicals and materials

Hydroxypropyl acrylate (HPA, 97%), trioctylphosphine (TOP, 97%), tetradecylphosphonic acid (TDPA, 97%), trioctylphosphine oxide (TOPO, 99%) were purchased from Strem Chemicals. Chloroform (99%), ethanol (99.8%), octane (99%), silver nanowires (Ag NWs, isopropyl alcohol suspension) were purchased from Sigma-Aldrich. Polydimethylsiloxane (PDMS, sylgard@184) was purchased from Dow. Cadmium oxide (CdO, 99.99%) was purchased from Aladdin.

2.2. Fabrication of the tactile perception system

The fabrication process of the tactile perception system began with the synthesis and purification of CdSe/CdS QRs, detailed in **Note S1**. Those QRs were first dispersed in an octane (10 mg mL^{-1}) solution. Later, this suspension was carefully mixed with PDMS in a volume ratio of 1:10. After stirring until they were well dispersed, the mixed suspension was drop cast onto the DVD mask, followed by a 24-hour drying process at room temperature. After the drying stage, Ag NWs suspension was spin-coated onto the QRs function added PDMS composite film to form a matrix serving as the electrode for the TENG on the surface. Once the Ag NWs electrode was in place, the whole film (size: 20 mm × 20 mm) was peeled off from the DVD mask, and one piece of the triboelectric sensor was successfully made. At last, an array consisting of eight triboelectric sensors was attached to two sides of the Fin Ray soft gripper (four sensors on each side) to form the tactile perception system for further applications.

2.3. Characterization

The energy-dispersive X-ray spectrum (EDX) was measured by a Zeiss EVO MA10 scanning electron microscope (SEM). The acceleration voltage was set to 5 kV. A Bruker X Flash 6–30 detector was applied to gain compositional information. Optical microscopy (OM) images were performed on an Axio Lab microscope (Carl Zeiss) in 10- and 50-fold magnification. The thicknesses of the prepared triboelectric layers were measured using a Bruker DektakXT Surface Profiler (2.5 μm tip radius). The transmittance spectra were obtained by a spectrophotometer (Lambda 35, PerkinElmer) with a scanning speed of 480 nm/min. Atomic force microscopy (AFM) images were acquired using an AFM instrument (MFP-3D, Asylum Research) in tapping mode. The output voltages and photocurrents of tactile sensors were measured by an electrometer (Keithley 6514) using a high impedance probe of 100 MΩ. The photoluminescence (PL) and absorbance spectrum were characterized by a spectrometer (HORIBA iHR550). The emission spectra at different stretching levels were obtained by a spectrometer (Ocean Optics HR2). Analog voltage signals were collected by the multichannel customized hardware circuit consisting of current amplifiers (LMC6001, Texas Instruments) and a micro-controller unit (Arduino Nano).

3. Results and discussion

3.1. Configuration of the triboelectric sensor

In this study, the silver nanowires (Ag NWs) matrix serves as the stretchable electrode for the single electrode-mode TENG-based triboelectric sensor. The dielectric layer of the TENG adopts a composite structure by adding CdSe/CdS QRs into a PDMS elastomer layer, together with a topography technology applied onto its surface. The successfully fabricated triboelectric sensor is schematically shown in Fig. 1**c**. The detailed fabrication process is described in Fig. S2. Transmittance characterization on the composite dielectric layer is shown in Fig. S3, demonstrating that added QRs are successfully incorporated in the film. Fig. S4 depicts the basic working mechanism of the single-electrode mode TENG, which is utilized in this work. First, because of the different capabilities of electron affinities, the equal density of positive and negative charges is generated on the contact surfaces of both PDMS composite film and the external object (i). Next, when the external object is located further away from the PDMS composite film (ii), the electrostatic induction effect causes electrons to flow from the bottom Ag NWs matrix electrode to the ground, driving the current I from the ground to the electrode, until getting the maximum distance (iii). After that, under the external pressing, the closer position of the external object to the PDMS composite film forces electrons to flow back from the ground to the bottom electrode (iv), which produces the reverse current $-I$. Finally, till the external object contacts the PDMS composite film again (i), a full working cycle of the single-electrode mode TENG to generate electrical signals is completed. In addition, our triboelectric sensor can be directly attached to different grippers attributed to its soft texture. With the ML technology, a triboelectric sensors-based tactile perception system can be successfully demonstrated to grasp and recognize different objects. Typical force and light signals collected by an MCU compositing the signal datasets in the ML algorithm are shown in Figs. 1**d** and 1**e**. The square-wave force signals can be acquired by our custom-made circuit, while the light signals are obtained from photoresistors integrated on both sides of the soft gripper. All channels of the analog signals generated from non-contact location detection and vertical contact force sensing first go through signal processing to be converted into digital signals before being transmitted to a terminal display, as shown in the diagram in Fig. 1**f**.

3.2. Output performance of TENG-based vertical force sensor

To verify the performance of TENG-based vertical force sensing capability, the custom-made force sensing measurement setup is built as shown in Fig. 2a, in which both pressing force and output voltage can be read simultaneously. Two different triboelectric sensors with and without imprinted structure (size: 20 mm × 20 mm) are fabricated for measuring their electrical outputs. As shown in Fig. S5a, the thicknesses of the prepared triboelectric layers are 647 μm. A DVD mask is used as the substrate for gaining imprinted structure on the surface of the PDMS composite film (Fig. S5b). The atomic force microscopy (AFM) image of the PDMS composite film with imprinted structure is shown in Fig. S5c. From its horizontal rectangle cut (Fig. S5d), the *ca.* 110 nm high wavy structure is seen on its surface. A comparison of output voltages between both structured triboelectric sensors is exemplified in Fig. S6. At the fixed distance of 10 mm and a slight pressing force of 2 N, the output voltages increase by 56.7% to 2.67 V. Figs. 2b and 2c display the output voltages of both structured triboelectric sensors at different pressing forces. Triboelectric sensors exhibit a two-stage sensing ability in Fig. 2d, which is independent of the surface structure. When the pressing force is lower than 4 N, the sensor reaches a very high resolution, while in the second region (pressing force $>$ 4 N), the sensitivity drops dramatically. The reason for the different sensing regions originates from the fact that the contact process between the external object and the PDMS composite film can also be divided into two states with increasing forces [48–50]. In the first state (red part), the increasing real contact area of the triboelectric sensor is the major factor for the increasing output voltages. The sensitivity enhancement of the imprinted structured triboelectric sensor is 28.0% (from 6.56 V N^{-1} to 8.40 V N^{-1}) in this stage, because the wavy structure on the surface gives more microscale elastic deformations for enlarging the real contact area between the external object and the PDMS composite film. In the

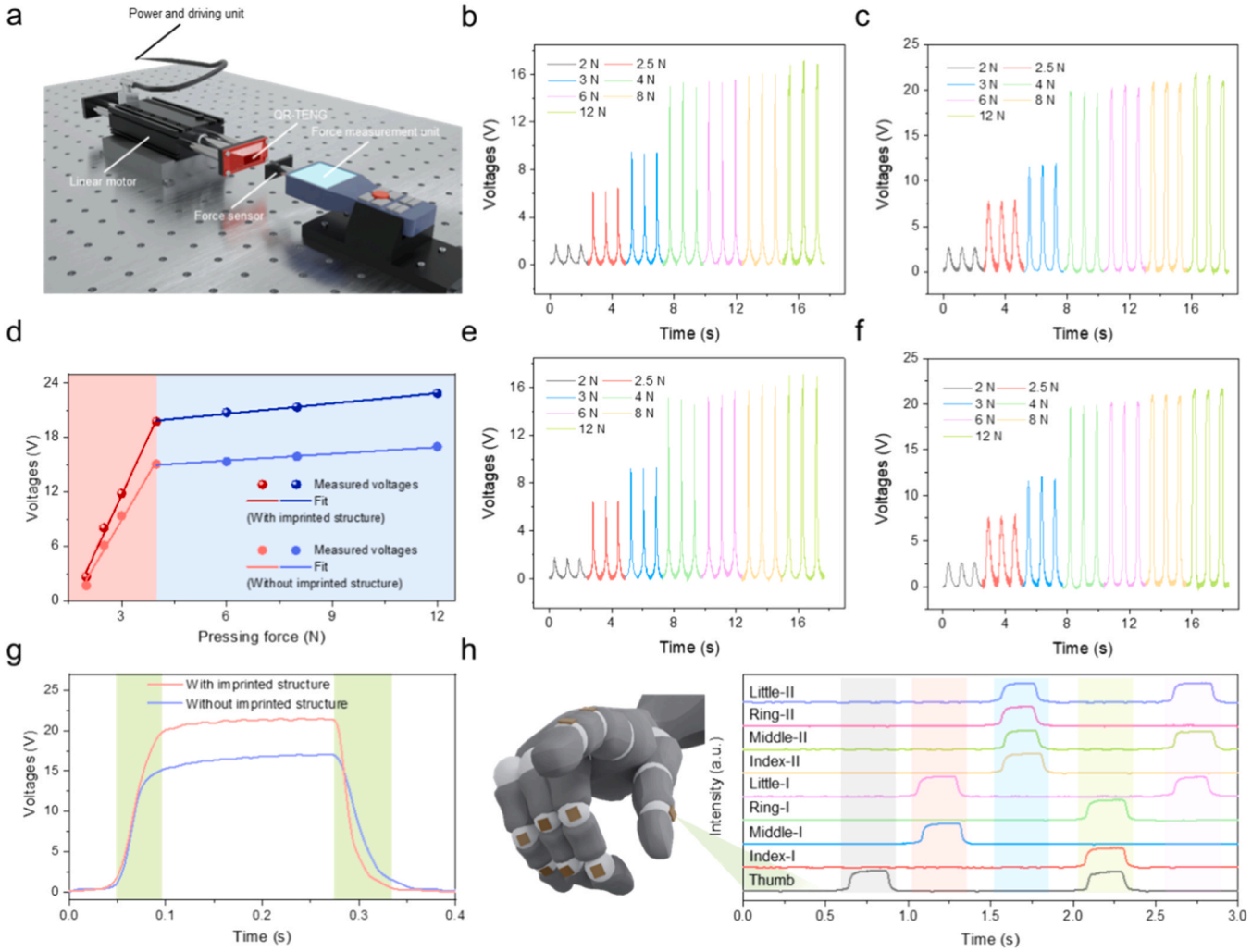

Fig. 2. Characterization of TENG based vertical force sensor. (a) Schematic illustration of the measurement setup for triboelectric sensors. (b-c) Output voltages of triboelectric sensors without and with imprinted structure at different pressing forces. (d) Output voltage peaks and related fits of two structural triboelectric sensors with increasing pressing forces. (e,f) Output voltages of triboelectric sensors without and with imprinted structure at different pressing forces under 100% lateral stretching levels. (g) Zoom-in signals of one-cycle outputs of two structural triboelectric sensors. (h) Diagram and output signals of imprinted triboelectric sensors integrated on a robotic hand under different touching conditions.

second period (blue part), the increasing contact area is caused by the elastic deformation of the PDMS composite film's soft texture itself, resulting in a slower enhancement of output voltages with increasing pressing forces. In this part, the effect of the imprinted structure becomes much weaker, and the sensitivity is only increased by 0.04 V N^{-1} to 0.29 V N^{-1} after applying topography technology on the surface. Fig. S7 shows that the outputs of the imprinted triboelectric sensor are stable and uniform under different pressing frequencies ranging from 0.32 Hz to 1.47 Hz. Moreover, to demonstrate the independence of vertical force sensing and lateral stretching degrees of our fabricated triboelectric sensors, we measure outputs of both structured triboelectric sensors under 100% (Figs. 2e and 2f) and 50% (Fig. S8a and S8b) stretching levels. Compared to the initial stretching levels, no obvious changes in output voltages at every measured force after stretching can be found, which shows that the triboelectric sensor exhibits almost consistent characteristics of output voltages under different lateral stretching levels. Typical one-cycle outputs of both structured triboelectric sensors are zoomed in Fig. 2**g**, from which response time (50 ms) and recovery time (80 ms) can be observed, indicating a fast response on vertical force sensing of our sensors. In addition, the output performance of the imprinted triboelectric sensor remains stable after 2000 working cycles (Fig. S9) and throughout 30 days of being exposed to ambient room conditions (Fig. S10), confirming its stability for long-time usage. Furthermore, as shown in Fig. 2**h**, vertical tactile sensing is also independent for nine triboelectric sensors-based pixels on a robotic hand. We can find corresponding responses from different pixels, which are generated under different touching conditions.

3.3. *Characterization of lateral tensile sensor*

We build the setup to characterize the lateral tensile sensing capability of our triboelectric sensor as sketched in Fig. 3a. In this setup, the triboelectric sensor is exposed to an ultraviolet light (365 nm) environment and can be stretched at different tensile strain degrees by a controlled linear motor. The lateral sensing ability of our triboelectric sensor is realized by adding CdSe/CdS QRs into the PDMS composite film. A photograph of the as-fabricated luminescent layer under ultraviolet light is shown in Fig. 3b. As the result of energy-dispersive X-ray (EDX) in Fig. 3c shows, added CdSe/CdS QRs are distributed in the composite film homogenously. Here, to enhance the conductivity for EDX measurements, gold (Au) is sputtered onto the surface of the composite film as a coating material. In this work, CdSe/CdS core-shell QRs are synthesized with a two-sequential seed-grown process, by which the emission and aspect ratio of the core-shell QRs are well controlled.

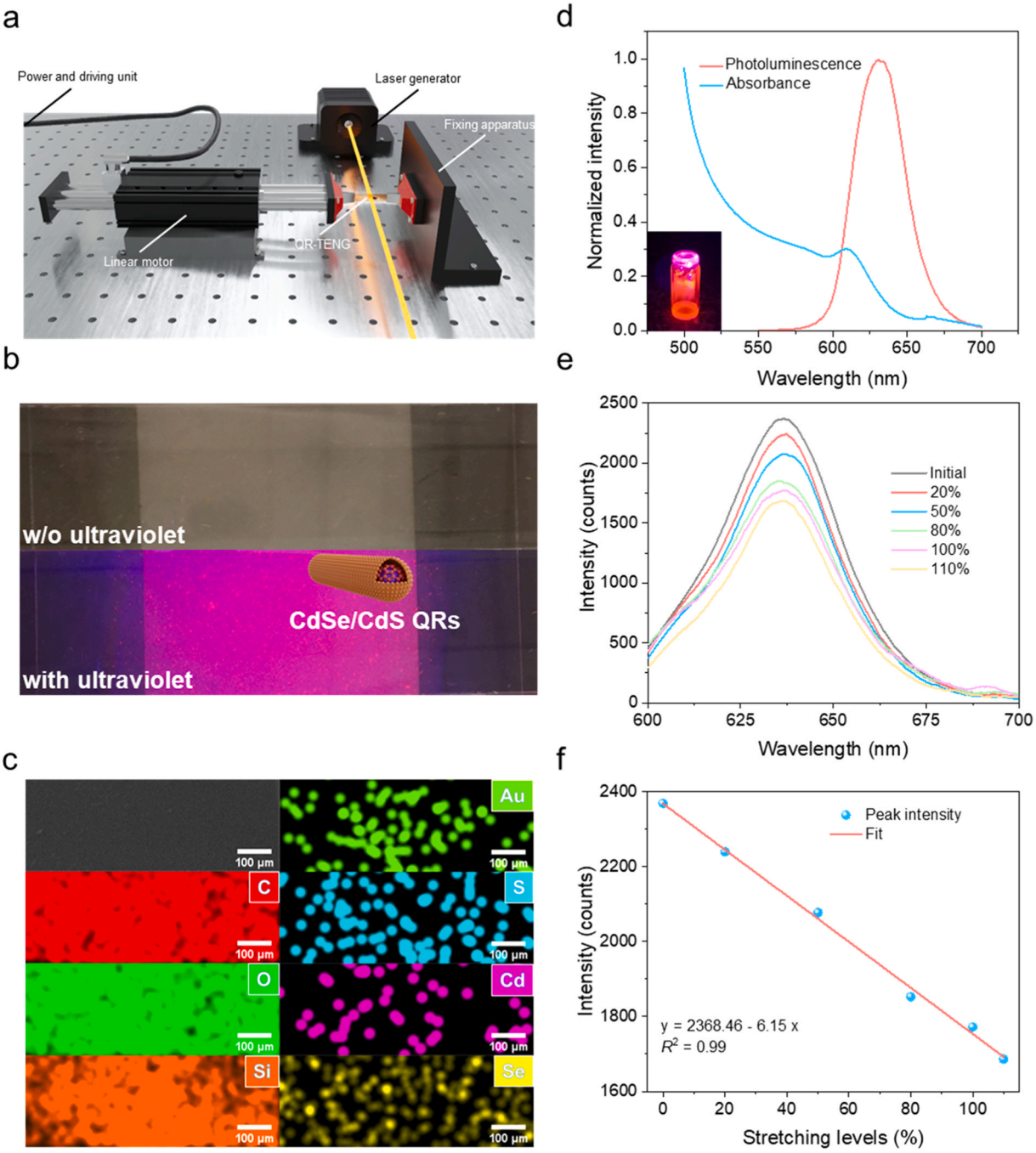

Fig. 3. Characterization of QRs based lateral stretching sensor. (a) Schematic illustration of the measurement setup for lateral stretching sensing. (b) Photographs of CdSe/CdS QRs function added luminescent layer with and without ultraviolet. (inset: diagram of the structure of QRs) (c) Energy-dispersive X-ray (EDX) spectrum of QRs function added PDMS composite film. (d) Photoluminescence and absorbance spectrum of synthesized QRs. (inset: photograph of QRs under ultraviolet) (e) Emission spectrum of QRs function added luminescent layer under ultraviolet at different stretching levels. (f) Intensity of peaks and related fit from QRs function added luminescent layer with increasing stretching levels.

The synthesis process is detailed in Note S1, which follows the recipe of our previous works [47,51]. Such fine-tuning could help attain high emission efficiency and enhance the dispersibility of nanoparticles within a PDMS matrix. The corresponding photoluminescence (PL) and absorbance spectrum of CdSe/CdS QRs are displayed in Fig. 3d. The emission intensities from the center part of the QRs function added luminescent PDMS composite layer at different tensile strain levels are shown in Fig. 3e. Fixed emission peaks at a wavelength of 635 nm are observed, which are generally consistent with that of CdSe/CdS QRs. Fig. 3f summarizes the intensity of the emission peak value, which decreases linearly with the higher stretching level of the triboelectric sensor with QRs functional addition. The linear fit result ($R^2 = 0.99$) shows that the device can reliably respond to stretching changes. Such a phenomenon is caused by a decrease in the density of CdSe/CdS QRs in the detection area with increasing stretching levels. To demonstrate the lateral sensing capability in real applications, we put a triboelectric sensor onto the inner-side joint of a robotic index finger with a photoresistor attached nearby. The photocurrent observed from the straightening process of the robotic index finger becomes gradually smaller (Fig. S11), which meets well the trend of the emission peak values at

different tensile degrees. Furthermore, as shown the photocurrent remains very stable during the lasting time of each state of the robotic finger.

3.4. Smart grasp with the ML technology

Outputs from both vertical force sensing and lateral tensile sensing of our triboelectric sensor show a good condition-dependent capability, which provides us with a two-dimensional sensing terminal. Enabled by its high sensitivity and stable output signals, we then utilize eight triboelectric sensors to form an array, and integrate this array on a Fin Ray soft gripper as the tactile perception system for smart grasp (Fig. 4a). Eight triboelectric sensors (named 'Force 1' to 'Force 8') and four photoresistors (named 'Light 1' to 'Light 4') as 12 signal channels are evenly distributed on both sides of the gripper, in which photoresistors are attached on the gripper for converting visualized light signals to computer-recognized electrical signals. In our ML-based smart grasp experiment, 18 objects with different materials and shapes are selected and grasped (Fig. 4b). Each object is grasped 50 times to enrich the signal datasets, and the collected 50 grasp samples are randomly split into training and testing groups with a ratio of 7:3 (training group: 35 samples; and testing group: 15 samples). As the duration time of the grasp process in a real application is also significant, we first design a new data acquisition circuit on the MCU platform for collecting multi-channel data generated by the TENGs (Fig. S12). As shown in Fig. 4c, in stark contrast to other reported works based on TENG [18,52], square-wave signals instead of pulse signals can be obtained on the MCU platform, which endows another feature in the ML algorithm. Fig. S13a shows the output signals of two force channels ('Force 1' and 'Force 5') on each side of the gripper as an example in our real grasp process. The robustness of our custom-made data acquisition circuit can be validated through its performance across over 900 working cycles in the smart grasp experiment. Notably, in a real grasp process, the grasp position has a big impact on output signals. For instance, as shown in Fig. 4d, when the gripper grasps a soft ball at the inner position, the outputs collected at 'Force 2' and 'Force 6' channels are the highest. In contrast, if the soft ball is grasped at the middle position, outputs from 'Force 2' and 'Force 6' channels become lower. When the grasp position moves outwards, 'Force 4' and 'Force 8' channels get the biggest values. This complex signal behavior for the same object in a random grasp process demonstrates the necessity of the ML technology for enabling a smarter grasp. In addition, the grasp orientation also influences the output signals during a real grasp task. The output signals obtained from grasping a soap at two different orientations are presented in Fig. S13b. However, it is essential to note that, due to the dimensional constraints of the soft gripper, there is a limit to the variation in the grasp orientations that can be applied to some chosen objects. Consequently, objects are predominantly grasped in a relatively uniform manner in this work. The output signals of all eight force channels generated from the grasp process of 18 objects are 3D-plotted in Fig. 4e. Schematic illustration of the ML technology utilized in our work is shown in Fig. 4f, which includes signals acquisition, datasets formation, training process by a neural network, and object recognition. The optimization process of the ML model is explained in Note S2. The Bidirectional Long Short-Term Memory (BiLSTM) neural network is finally chosen in this study owing to the advantages of handling learning tasks such as classification and prediction based on a complete input sequence. The confusion maps of prediction trained by only TENG based force signals on 18 objects are visualized in Fig. S14. Compared with the outcome in Fig. S14a, Fig. S14b shows that although the number of force channels is the same (four signal channels), a more diverse setting of triboelectric sensors on the gripper is beneficial for improving the test accuracy. According to the confusion map in Fig. S14c, the accuracy of the prediction outcome has the highest value of 96.3% among these confusion maps trained by TENG based force signals. It can be clearly observed that more sensing channels provide more useful data, and thus lead to a more effective training dataset to create a higher accuracy. However, it needs to be emphasized that for a certain gripper, normally the amount of free space limits the number of sensors. Thus, in addition to the reduction of the sensor size, making our sensor multi-dimensional is another pathway for a more desirable result. To achieve this, output signals in relation to lateral stretching sensing capability are collected as another feature for ML training. 3D plots of light signals from tactile perception systems corresponding to 18 objects are drawn in Fig. S15a. Fig. S15b provides a detailed mechanism diagram that shows the role of light signals that are collected via the MCU platform during the object recognition process. The diagram reveals that the light signal is a composite result of two primary factors: emission intensity variations due to the triboelectric sensor's deformation from both stretching and compressing and the extent of light occlusion, which is directly related to the shadow area blocked by different objects when grasping. The confusion map of prediction with four light signals on 18 objects shows the test accuracy of 94.1% (Fig. S16). By combining all signals from eight force and four light channels, the best accuracy of 98.5% can be achieved (Fig. 4g), demonstrating a high resolution of object recognition in our tactile perception system based smart grasp process. Additionally, as illustrated in Fig. 4h, after 40 times of training cycles, the training recognition accuracy obtained by both two kinds of signal channels can gradually reach 99.8%. This improvement demonstrates that light signals can be incorporated well to assist the recognition for a better result. Moreover, it needs to be noted that the ability to generalize and the accuracy of the ML model could be further enhanced by a larger sample size of the chosen objects for training.

3.5. Intelligent sorting without seeing

To show the practical application of our tactile perception system, an intelligent sorting system is built with a robotic arm as sketched in Fig. 5a. It is shown that the process flow for an intelligent sorting system includes objects' finding, grasp, recognition, and finally delivery. We find that, when a charged object comes closer to our tactile perception system before any physical contact, a clear wave signal which is inversely proportional to the distance can be observed by our custom-made circuit (Fig. S17). It can be interpreted by the electrostatic induction effect, where the varying electric field introduced by the external object causes the collected output signals. Note that, most objects in our daily life carry charges naturally owing to contact electrification [53], which means that through our customized data acquisition circuit, objects can be detected on the MCU platform even before grasp. In this work, the bottom two triboelectric sensors on the gripper ('Force 4' and 'Force 8') play the role of electroreceptors for object detection in the intelligent sorting system, and the maximum distance between two symmetrical electroreceptors is fixed at 10 cm. One electroreceptor on each side of the gripper in this system is used to eliminate distractions from the electric fields of other objects and confirm the object locating in the middle of two sides of the gripper for further accurate grasp. When the computer-controlled robotic arm drives the gripper to cruise on the surface of a clean experimental table, the output signals of both detectors remain very stable (Fig. S18a). After we put some objects on the table, different signal peaks appear when the robotic arm scans through them (Fig. S18b, S18c, and S18d), showing its ability to detect the object's location. Then, we arrange 'Apple', 'Wafer', and 'Can' in a row (Fig. S19a) on the table for a robotic arm scan process, and the voltage signals collected by two electroreceptors are shown in Fig. S19b. Obvious signal peaks are generated, which refer to corresponding locations of the different objects (Movie S1). Finally, the whole system is placed under ultraviolet light conditions for the 'without seeing' intelligent sorting. We divide the whole experimental table into eight areas, and the gripper scans through them to look for the objects. It means that the object state is binary (presence or absence) in each area. The categories of 'Food', 'Drink', and 'Others' are labeled on boxes respectively for the final delivery. In the scan process, if there are obvious signals on

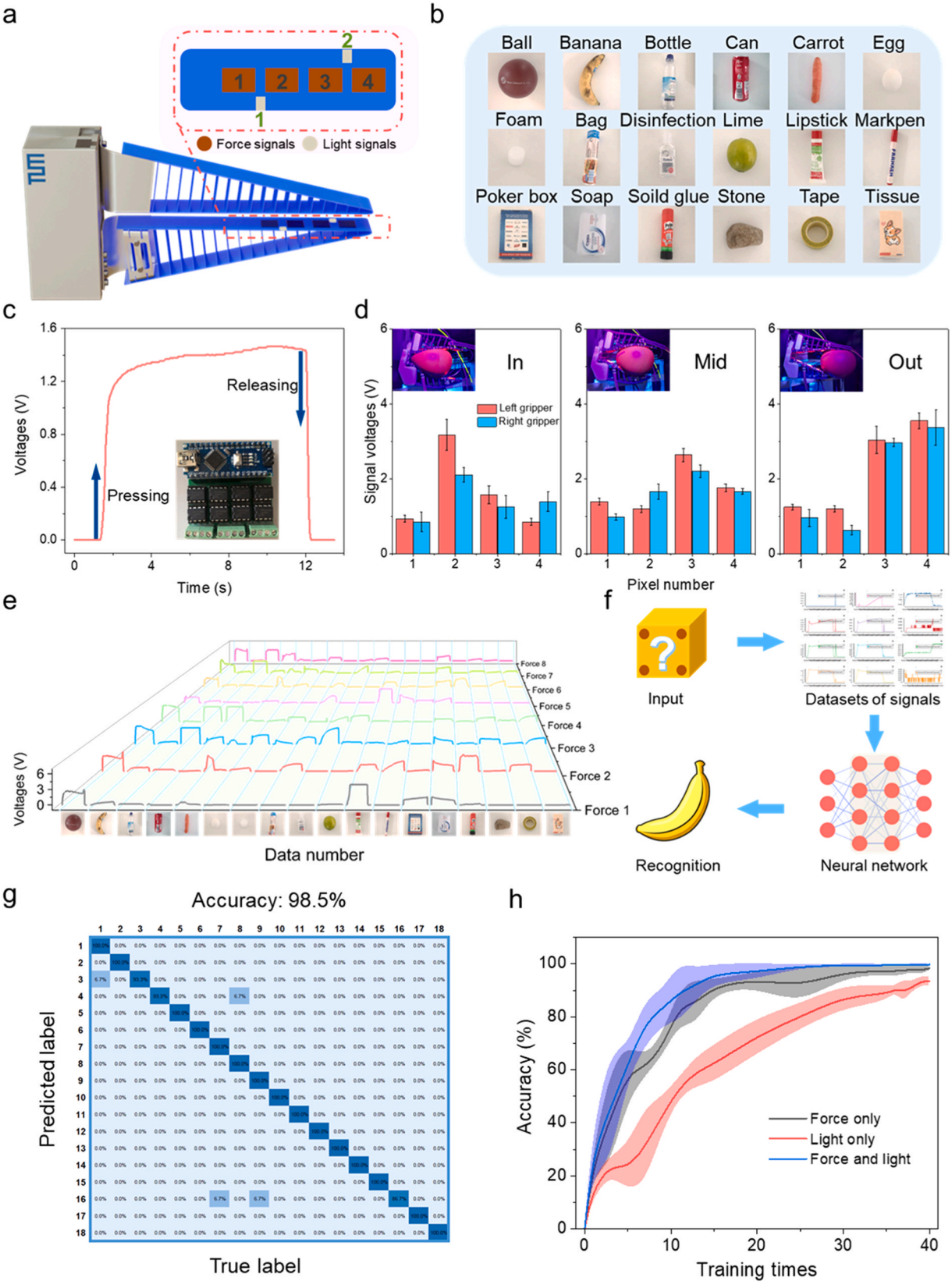

Fig. 4. Smart grasp by the tactile perception system. (a) Channel arrangements of the soft gripper integrated with the triboelectric sensors. (b) 18 objects to be grasped and recognized. (c) Typical square-wave signals collected by the designed circuit. (inset: circuit board integrated with an Arduino Nano and eight current amplifiers for multichannel data collection) (d) Output force signals of tactile perception system for grasping a soft ball at various contact positions. (e) 3D plots of output voltage signals from eight force channels corresponding to different objects. (f) Schematic illustration of components of the recognition system, including signals collection, datasets formation, training by a neural network, and classification. (g) Confusion map of prediction with eight force and four light signals on 18 objects. (h) Training recognition accuracy with increasing training times.

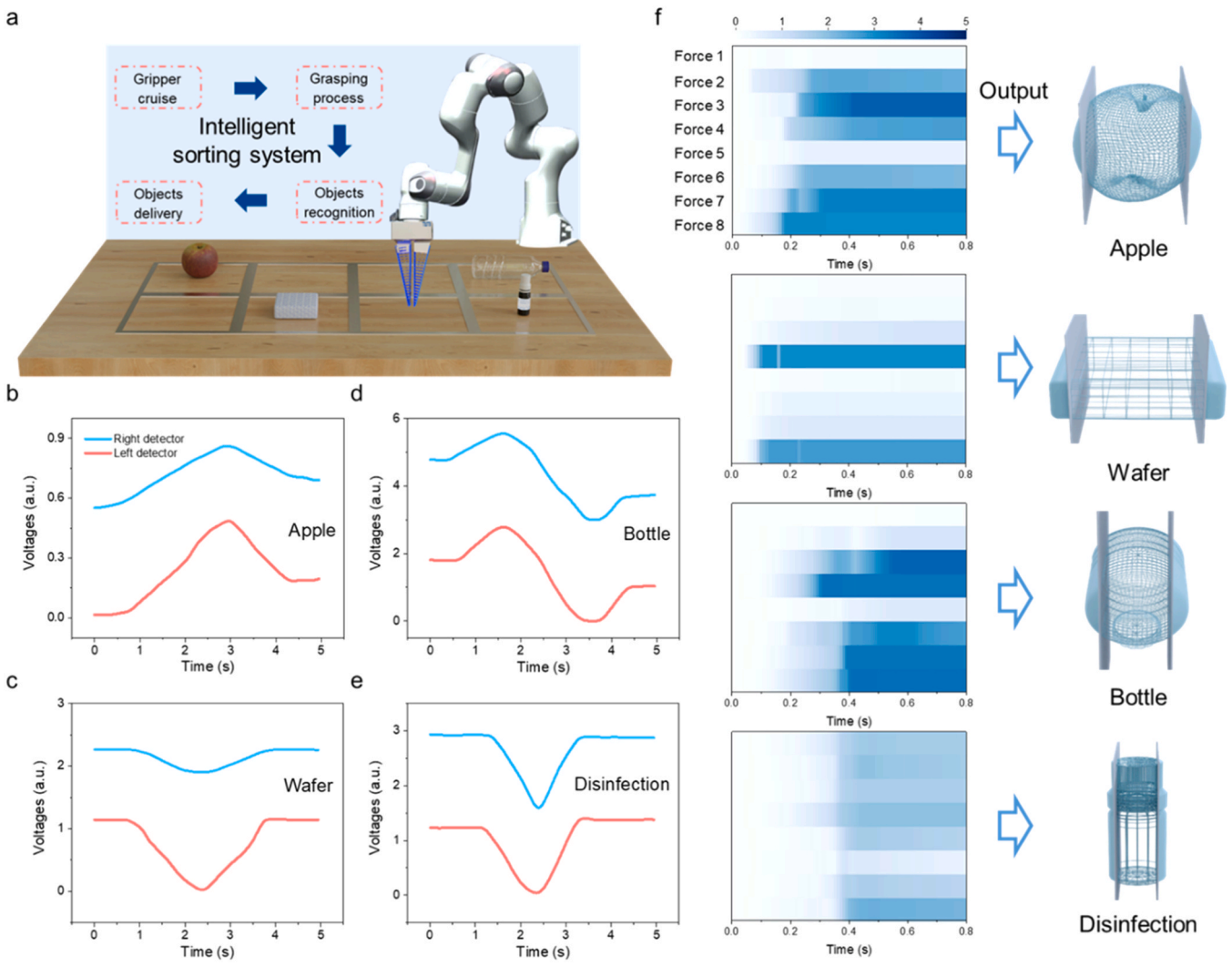

Fig. 5. Real-time intelligent sorting without seeing. (a) Diagram and process flow of the real-time intelligent sorting without seeing by controlling a robotic arm with ML technology. (b) Non-contact electrical signals generated by 'Apple' during the real-time scan process. (c) Non-contact electrical signals generated by 'Wafer' during the real-time scan process. (d) Non-contact electrical signals generated by 'Bottle' during the real-time scan process. (e) Non-contact electrical signals generated by 'Disinfection' during the real-time scan process. (f) Every moment of signals from eight force channels when grasping 'Apple', 'Wafer', 'Bottle', and 'Disinfection' and their recovery results in the virtual environment.

both electroreceptors, the computer will mark this position for later grasp by the gripper, otherwise this position will be skipped automatically. Moreover, in our controlling system, we set a high threshold of induced signal for the object detection, which ensures that our system's response could be more definitive and precise. The location detection and object recognition results for 'Apple' (Fig. 5b and Fig. S20), 'Wafer' (Fig. 5c and Fig. S21), 'Bottle' (Fig. 5d and Fig. S22), and 'Disinfection' (Fig. 5e and Fig. S23) are respectively illustrated. Within only 0.8 seconds, highly accurate object recognition can be achieved by every moment of force and light signals from each channel (Fig. 5f). Every object is successfully recovered in a virtual environment by its unique characteristics. 'Apple', 'Wafer', 'Bottle', and 'Disinfection' are all delivered into right boxes (Fig. S24 and Movie S2), which displays the great potential applications of our triboelectric sensors-based tactile perception system. Here, to further demonstrate the versatility of our intelligent sorting system at room conditions, we also built another scene with different objects and placements for testing, and the result is shown in Movie S3. Additionally, further sterilization of objects is possible through the use of ultraviolet light conditions, which is beneficial to prevent the reproduction of bacteria. Finally, environmental parameters such as temperature and humidity can indeed affect the output performance or stability of triboelectric sensors, leading to negative impacts on sensing accuracy [54,55]. Hence, encapsulation techniques could be considered in severe environments to create a barrier against ambient environmental changes, thereby stabilizing the sensor's performance in practical applications.

Supplementary material related to this article can be found online at doi:10.1016/j.nanoen.2024.109398.

4. Conclusions

In summary, we developed a multi-dimensional tactile perception system for smart grasp with the ML technology. Besides the TENG based vertical force sensing, the variable luminescent effect carried by the functional addition of CdSe/CdS QRs is introduced in our triboelectric sensor for lateral tensile sensing. After applying an artificial surface structure, a 28.0% enhancement of the force-sensing resolution is achieved. In addition, the robustness and independent sensing capability of the fabricated triboelectric sensor are demonstrated in our work. By integrating eight triboelectric sensors-based arrays on a soft gripper, the formed tactile perception system successfully grasps and recognizes different 18 objects with an accuracy of 96.3% relying on force signals,

which can be further enhanced to 98.5% with the aid of light signals. Furthermore, we design a 'without seeing' intelligent sorting system based on our tactile perception system. Compared to other state-of-the-art reported counterparts, our intelligent sorting does not require any external apparatus for location detection. With a further potential sterilization originating from ultraviolet light, it meets the demands for more intelligent and energy-saving sorting in both smart home and smart factory applications.

CRediT authorship contribution statement

Guo Renjun: Writing – review & editing, Methodology, Investigation. **Tu Suo:** Writing – review & editing, Methodology, Investigation. **Pan Guangjiu:** Writing – review & editing, Methodology. **Guan Tianfu:** Writing – review & editing, Methodology. **Wang Kai:** Writing – review & editing, Supervision. **Xiao Tianxiao:** Writing – original draft, Visualization, Methodology, Investigation, Data curation, Conceptualization. **Sun Xiao Wei:** Writing – review & editing, Supervision. **Bing Zhenshan:** Writing – review & editing, Methodology, Investigation, Data curation, Conceptualization. **Huang Kai:** Writing – review & editing, Supervision. **Wu Yansong:** Writing – review & editing, Methodology, Investigation. **Knoll Alois:** Writing – review & editing, Supervision. **Chen Wei:** Writing – review & editing, Methodology, Investigation. **Wang Zhong Lin:** Writing – review & editing, Supervision, Project administration, Conceptualization. **Zhou Ziming:** Writing – review & editing, Methodology, Investigation. **Mueller-Buschbaum Peter:** Writing – review & editing, Supervision, Project administration, Conceptualization. **Fang Fan:** Writing – review & editing, Methodology, Investigation. **Liang Suzhe:** Writing – review & editing, Visualization, Methodology.

Declaration of Competing Interest

The authors declare that they have no known competing financial interests or personal relationships that could have appeared to influence the work reported in this paper.

Data availability

Data will be made available on request.

Acknowledgement

This work is supported by funding from the Deutsche Forschungsgemeinschaft (DFG, German Research Foundation) via Germany's Excellence Strategy–EXC 2089/1–390776260 (e-conversion) and *via* the International Research Training Group 2022 Alberta/Technical University of Munich International Graduate School for Environmentally Responsible Functional Hybrid Materials (ATUMS), TUM.solar in the context of the Bavarian Collaborative Research Project Solar Technologies Go Hybrid (SolTech), the Center for NanoScience (CeNS), the European Union's Horizon 2020 Framework Programme for Research and Innovation under the Specific Grant Agreement No. 945539 (Human Brain Project SGA3), Key-Area Research and Development of Guangdong Province No. 2020B0101650001, Science and Technology Planning Project of Guangzhou city of China No. 202007050004, and Pazhou Lab No. PZL2021KF0020. W.C. acknowledges the funding support from the National Natural Science Foundation of China No. 12204318 and the Guangdong Basic and Applied Basic Research Foundation No. 2021A1515110535. We also acknowledge financial support from the Chinese Scholarship Council (CSC) and thank Prof. Alexander Holleitner and Peter Weiser for providing access to the AFM measurements.

Appendix A. Supporting information

Supplementary data associated with this article can be found in the online version at doi:10.1016/j.nanoen.2024.109398.

References

[1] M. Venus, J. Waterman, I. McNab, Basic physiology of the skin, Surgery 28 (2010) 469–472, https://doi.org/10.1016/j.mpsur.2010.07.011.
[2] M. Sand, T. Gambichler, D. Sand, M. Skrygan, P. Altmeyer, F.G. Bechara, MicroRNAs and the skin: tiny players in the body's largest organ, J. Dermatol. Sci. 53 (2009) 169–175, https://doi.org/10.1016/j.jdermsci.2008.10.004.
[3] H.H. Chou, A. Nguyen, A. Chortos, J.W.F. To, C. Lu, J. Mei, T. Kurosawa, W.G. Bae, J.B.H. Tok, Z. Bao, A chameleon-inspired stretchable electronic skin with interactive colour changing controlled by tactile sensing, Nat. Commun. 6 (2015) 8011, https://doi.org/10.1038/ncomms9011.
[4] J. Park, D.H. Kang, H. Chae, S.K. Ghosh, C. Jeong, Y. Park, S. Cho, Y. Lee, J. Kim, Y. Ko, J.J. Kim, H. Ko, Frequency-selective acoustic and haptic smart skin for dual-mode dynamic/static human-machine interface, Sci. Adv. 8 (2022) eabj9220, https://doi.org/10.1126/sciadv.abj9220.
[5] Y. Luo, Y. Li, P. Sharma, W. Shou, K. Wu, M. Foshey, B. Li, T. Palacios, A. Torralba, W. Matusik, Learning human–environment interactions using conformal tactile textiles, Nat. Electron. 4 (2021) 193–201, https://doi.org/10.1038/s41928-021-00558-0.
[6] T. Bu, T. Xiao, Z. Yang, G. Liu, X. Fu, J. Nie, T. Guo, Y. Pang, J. Zhao, F. Xi, C. Zhang, Z.L. Wang, Stretchable triboelectric–photonic smart skin for tactile and gesture sensing, Adv. Mater. 30 (2018) 1800066, https://doi.org/10.1002/adma.201800066.
[7] S. Sundaram, P. Kellnhofer, Y. Li, J.Y. Zhu, A. Torralba, W. Matusik, Learning the signatures of the human grasp using a scalable tactile glove, Nature 569 (2019) 698–702, https://doi.org/10.1038/s41586-019-1234-z.
[8] Y. Lu, H. Tian, J. Cheng, F. Zhu, B. Liu, S. Wei, L. Ji, Z.L. Wang, Decoding lip language using triboelectric sensors with deep learning, Nat. Commun. 13 (2022) 1401, https://doi.org/10.1038/s41467-022-29083-0.
[9] Z. Wen, Y. Yang, N. Sun, G. Li, Y. Liu, C. Chen, J. Shi, L. Xie, H. Jiang, D. Bao, Q. Zhuo, X. Sun, A wrinkled PEDOT:PSS film based stretchable and transparent triboelectric nanogenerator for wearable energy harvesters and active motion sensors, Adv. Funct. Mater. 28 (2018) 1803684, https://doi.org/10.1002/adfm.201803684.
[10] Z. Zhou, K. Chen, X. Li, S. Zhang, Y. Wu, Y. Zhou, K. Meng, C. Sun, Q. He, W. Fan, E. Fan, Z. Lin, X. Tan, W. Deng, J. Yang, J. Chen, Sign-to-speech translation using machine-learning-assisted stretchable sensor arrays, Nat. Electron. 3 (2020) 571–578, https://doi.org/10.1038/s41928-020-0428-6.
[11] Y. Jiang, Z. Zhang, Y.X. Wang, D. Li, C.T. Coen, E. Hwaun, G. Chen, H.C. Wu, D. Zhong, S. Niu, W. Wang, A. Saberi, J.C. Lai, Y. Wu, Y. Wang, A.A. Trotsyuk, K. Y. Loh, C.C. Shih, W. Xu, K. Liang, K. Zhang, Y. Bai, G. Gurusankar, W. Hu, W. Jia, Z. Cheng, R.H. Dauskardt, G.C. Gurtner, J.B.H. Tok, K. Deisseroth, I. Soltesz, Z. Bao, Topological supramolecular network enabled high-conductivity, stretchable organic bioelectronics, Science 375 (2022) 1411–1417, https://doi.org/10.1126/science.abj7564.
[12] W. Asghar, F. Li, Y. Zhou, Y. Wu, Z. Yu, S. Li, D. Tang, X. Han, J. Shang, Y. Liu, R. W. Li, Piezocapacitive flexible e-skin pressure sensors having magnetically grown microstructures, Adv. Mater. Technol. 5 (2020) 1900934, https://doi.org/10.1002/admt.201900934.
[13] Y.H. Jung, J.Y. Yoo, A. Vázquez-Guardado, J.H. Kim, J.T. Kim, H. Luan, M. Park, J. Lim, H.S. Shin, C.J. Su, R. Schloen, J. Trueb, R. Avila, J.K. Chang, D.S. Yang, Y. Park, H. Ryu, H.J. Yoon, G. Lee, H. Jeong, J.U. Kim, A. Akhtar, J. Cornman, T. Kim, Y. Huang, J.A. Rogers, A wireless haptic interface for programmable patterns of touch across large areas of the skin, Nat. Electron. 5 (2022) 374–385, https://doi.org/10.1038/s41928-022-00765-3.
[14] A. Moin, A. Zhou, A. Rahimi, A. Menon, S. Benatti, G. Alexandrov, S. Tamakloe, J. Ting, N. Yamamoto, Y. Khan, F. Burghardt, L. Benini, A.C. Arias, J.M. Rabaey, A wearable biosensing system with in-sensor adaptive machine learning for hand gesture recognition, Nat. Electron. 4 (2021) 54–63, https://doi.org/10.1038/s41928-020-00510-8.
[15] P. Sahatiya, S. Badhulika, Eraser-based eco-friendly fabrication of a skin-like large-area matrix of flexible carbon nanotube strain and pressure sensors, Nanotechnology 28 (2017) 095501, https://doi.org/10.1088/1361-6528/aa5845.
[16] G. Schwartz, B.C.K. Tee, J. Mei, A.L. Appleton, D.H. Kim, H. Wang, Z. Bao, Flexible polymer transistors with high pressure sensitivity for application in electronic skin and health monitoring, Nat. Commun. 4 (2013) 1859, https://doi.org/10.1038/ncomms2832.
[17] D.J. Lipomi, M. Vosgueritchian, B.C.K. Tee, S.L. Hellstrom, J.A. Lee, C.H. Fox, Z. Bao, Skin-like pressure and strain sensors based on transparent elastic films of carbon nanotubes, Nat. Nanotechnol. 6 (2011) 788–792, https://doi.org/10.1038/nnano.2011.184.
[18] T. Jin, Z. Sun, L. Li, Q. Zhang, M. Zhu, Z. Zhang, G. Yuan, T. Chen, Y. Tian, X. Hou, C. Lee, Triboelectric nanogenerator sensors for soft robotics aiming at digital twin applications, Nat. Commun. 11 (2020) 5381, https://doi.org/10.1038/s41467-020-19059-3.
[19] Q. Zheng, M. Peng, Z. Liu, S. Li, R. Han, H. Ouyang, Y. Fan, C. Pan, W. Hu, J. Zhai, Z. Li, Z.L. Wang, Dynamic real-time imaging of living cell traction force by piezo-phototronic light nano-antenna array, Sci. Adv. 7 (2021) abe7738, https://doi.org/10.1126/sciadv.abe7738.

[20] L. Wang, Z. Lou, K. Wang, S. Zhao, P. Yu, W. Wei, D. Wang, W. Han, K. Jiang, G. Shen, Biocompatible and biodegradable functional polysaccharides for flexible humidity sensors, Research 2020 (2020) 8716847, https://doi.org/10.34133/2020/8716847.
[21] Y. Li, S. Xiao, X. Zhang, P. Jia, S. Tian, C. Pan, F. Zeng, D. Chen, Y. Chen, J. Tang, J. Xiong, Silk inspired in-situ interlocked superelastic microfibers for permeable stretchable triboelectric nanogenerator, Nano Energy 98 (2022) 107347, https://doi.org/10.1016/j.nanoen.2022.107347.
[22] H. Guo, C. Lan, Z. Zhou, P. Sun, D. Wei, C. Li, Transparent, flexible, and stretchable WS_2 based humidity sensors for electronic skin, Nanoscale 9 (2017) 6246–6253, https://doi.org/10.1039/C7NR01016H.
[23] G. Liu, Q. Tan, H. Kou, L. Zhang, J. Wang, W. Lv, H. Dong, J. Xiong, A flexible temperature sensor based on reduced graphene oxide for robot skin used in internet of things, Sensors 18 (2018) 1400, https://doi.org/10.3390/s18051400.
[24] S.Y. Hong, Y.H. Lee, H. Park, S.W. Jin, Y.R. Jeong, J. Yun, I. You, G. Zi, J.S. Ha, Stretchable active matrix temperature sensor array of polyaniline nanofibers for electronic skin, Adv. Mater. 28 (2016) 930–935, https://doi.org/10.1002/adma.201504659.
[25] M. Ha, G.S.C. Bermúdez, T. Kosub, I. Mönch, Y. Zabila, E.S.O. Mata, R. Illing, Y. Wang, J. Fassbender, D. Makarov, Printable and stretchable giant magnetoresistive sensors for highly compliant and skin-conformal electronics, Adv. Mater. 33 (2021) 2005521, https://doi.org/10.1002/adma.202005521.
[26] G.S.C. Bermúdez, D.D. Karnaushenko, D. Karnaushenko, A. Lebanov, L. Bischoff, M. Kaltenbrunner, J. Fassbender, O.G. Schmidt, D. Makarov, Magnetosensitive e-skins with directional perception for augmented reality, Sci. Adv. 4 (2018) eaao2623, https://doi.org/10.1126/sciadv.aao2623.
[27] Y. Zhang, J. Zhou, Y. Zhang, D. Zhang, K.T. Yong, J. Xiong, Elastic fibers/fabrics for wearables and bioelectronics, Adv. Sci. 9 (2022) 2203808, https://doi.org/10.1002/advs.202203808.
[28] S.J. Starr, C.E. Metz, L.B. Lusted, D.J. Goodenough, Visual detection and localization of radiographic images, Radiology 116 (1975) 533–538, https://doi.org/10.1148/116.3.533.
[29] H. Hu, H. Huang, M. Li, X. Gao, L. Yin, R. Qi, R.S. Wu, X. Chen, Y. Ma, K. Shi, C. Li, T.M. Maus, B. Huang, C. Lu, M. Lin, S. Zhou, Z. Lou, Y. Gu, Y. Chen, Y. Lei, X. Wang, R. Wang, W. Yue, X. Yang, Y. Bian, J. Mu, G. Park, S. Xiang, S. Cai, P. W. Corey, J. Wang, S. Xu, A wearable cardiac ultrasound imager, Nature 613 (2023) 667–675, https://doi.org/10.1038/s41586-022-05498-z.
[30] O. Couture, V. Hingot, B. Heiles, P. Muleki-Seya, M. Tanter, Ultrasound localization microscopy and super-resolution: a state of the art, IEEE Trans. Ultrason. Ferroelectr. Freq. Control 65 (2018) 1304–1320, https://doi.org/10.1109/TUFFC.2018.2850811.
[31] G.A. Howland, P.B. Dixon, J.C. Howell, Photon-counting compressive sensing laser radar for 3D imaging, Appl. Opt. 50 (2011) 5917–5920, https://doi.org/10.1364/AO.50.005917.
[32] J.D. Pettigrew, Electroreception in monotremes, J. Exp. Biol. 202 (1999) 1447–1454, https://doi.org/10.1242/jeb.202.10.1447.
[33] F.R. Fan, Z.Q. Tian, Z.L. Wang, Flexible triboelectric generator, Nano Energy 1 (2012) 328–334, https://doi.org/10.1016/j.nanoen.2012.01.004.
[34] Z.L. Wang, On Maxwell's displacement current for energy and sensors: the origin of nanogenerators, Mater. Today 20 (2017) 74–82, https://doi.org/10.1016/j.mattod.2016.12.001.
[35] Z.L. Wang, A.C. Wang, On the origin of contact-electrification, Mater. Today 30 (2019) 34–51, https://doi.org/10.1016/j.mattod.2019.05.016.
[36] Y.C. Lai, H.M. Wu, H.C. Lin, C.L. Chang, H.H. Chou, Y.C. Hsiao, Y.C. Wu, Entirely, intrinsically, and autonomously self-healable, highly transparent, and superstretchable triboelectric nanogenerator for personal power sources and self-powered electronic skins, Adv. Funct. Mater. 29 (2019) 1904626, https://doi.org/10.1002/adfm.201904626.
[37] H.J. Qiu, W.Z. Song, X.X. Wang, J. Zhang, Z. Fan, M. Yu, S. Ramakrishna, Y. Z. Long, A calibration-free self-powered sensor for vital sign monitoring and finger tap communication based on wearable triboelectric nanogenerator, Nano Energy 58 (2019) 536–542, https://doi.org/10.1016/j.nanoen.2019.01.069.
[38] Z. Li, Q. Zheng, Z.L. Wang, Z. Li, Nanogenerator-based self-powered sensors for wearable and implantable electronics, Research 2020 (2020) 8710686, https://doi.org/10.34133/2020/8710686.
[39] Y. Song, J. Min, Y. Yu, H. Wang, H. Zhang, W. Gao, Wireless battery-free wearable sweat sensor powered by human motion, Sci. Adv. 6 (2020) eaay9842, https://doi.org/10.1126/sciadv.aay9842.
[40] J. An, P. Chen, Z. Wang, A. Berbille, H. Pang, Y. Jiang, T. Jiang, Z.L. Wang, Biomimetic hairy whiskers for robotic skin tactility, Adv. Mater. 33 (2021) 2101891, https://doi.org/10.1002/adma.202101891.
[41] M. He, W. Du, Y. Feng, S. Li, W. Wang, X. Zhang, A. Yu, L. Wan, J. Zhai, Flexible and stretchable triboelectric nanogenerator fabric for biomechanical energy harvesting and self-powered dual-mode human motion monitoring, Nano Energy 86 (2021) 106058, https://doi.org/10.1016/j.nanoen.2021.106058.
[42] X. Zhang, Z. Li, W. Du, Y. Zhao, W. Wang, L. Pang, L. Chen, A. Yu, J. Zhai, Self-powered triboelectric-mechanoluminescent electronic skin for detecting and differentiating multiple mechanical stimuli, Nano Energy 96 (2022) 107115, https://doi.org/10.1016/j.nanoen.2022.107115.
[43] M. Kazes, D.Y. Lewis, Y. Ebenstein, T. Mokari, U. Banin, Lasing from semiconductor quantum rods in a cylindrical microcavity, Adv. Mater. 14 (2002) 317–321, https://doi.org/10.1002/1521-4095(20020219)14:4<317::AID-ADMA317>3.0.CO;2-U.
[44] F. Di Stasio, J.Q. Grim, V. Lesnyak, P. Rastogi, L. Manna, I. Moreels, R. Krahne, Single-mode lasing from colloidal water-soluble CdSe/CdS quantum dot-in-rods, Small 11 (2015) 1328–1334, https://doi.org/10.1002/smll.201402527.
[45] A. Singh, X. Li, V. Protasenko, G. Galantai, M. Kuno, H. Xing, D. Jena, Polarization-sensitive nanowire photodetectors based on solution-synthesized CdSe quantum-wire solids, Nano Lett. 7 (2007) 2999–3006, https://doi.org/10.1021/nl0713023.
[46] Y. Chen, W. Xing, Y. Liu, X. Zhang, Y. Xie, C. Shen, J.G. Liu, C. Geng, S. Xu, Efficient and stable CdSe/CdS/ZnS quantum rods-in-matrix assembly for white LED application, Nanomaterials 10 (2020) 317, https://doi.org/10.3390/nano10020317.
[47] Z. Zhou, K. Wang, Z. Zhang, C. Zhang, H. Liu, Y. Zhang, Z. Wen, S. Li, J. Hao, B. Xu, S.J. Pennycook, K.L. Teo, X.W. Sun, Highly polarized fluorescent film based on aligned quantum rods by contact ink-jet printing method, IEEE Photonics J. 11 (2019) 1–11, https://doi.org/10.1109/JPHOT.2019.2902313.
[48] M. Ha, S. Lim, S. Cho, Y. Lee, S. Na, C. Baig, H. Ko, Skin-inspired hierarchical polymer architectures with gradient stiffness for spacer-free, ultrathin, and highly sensitive triboelectric sensors, ACS Nano 12 (2018) 3964–3974, https://doi.org/10.1021/acsnano.8b01557.
[49] K. Meng, J. Chen, X. Li, Y. Wu, W. Fan, Z. Zhou, Q. He, X. Wang, X. Fan, Y. Zhang, J. Yang, Z.L. Wang, Flexible weaving constructed self-powered pressure sensor enabling continuous diagnosis of cardiovascular disease and measurement of cuffless blood pressure, Adv. Funct. Mater. 29 (2018) 1806388, https://doi.org/10.1002/adfm.201806388.
[50] Y. Zhong, J. Wang, L. Han, S. Dai, H. Zhu, J. Hua, G. Cheng, J. Ding, High-performance flexible self-powered triboelectric pressure sensor based on chemically modified micropatterned PDMS film, Sens. Actuator A Phys. 349 (2023) 114013, https://doi.org/10.1016/j.sna.2022.114013.
[51] Y. Yang, J. Li, H. Liu, Z. Zhou, J. Li, J. Huang, Z. Zhang, Y. Zhang, H. Dai, K. Wang, X.W. Sun, J. Yao, Enhanced frequency and amplitude modulation of THz metasurfaces based on CdSe/CdS quantum rods, Opt. Commun. 471 (2020) 126014, https://doi.org/10.1016/j.optcom.2020.126014.
[52] J.K. Han, I.W. Tcho, S.B. Jeon, J.M. Yu, W.G. Kim, Y.K. Choi, Self-powered artificial mechanoreceptor based on triboelectrification for a neuromorphic tactile system, Adv. Sci. 9 (2022) 2105076, https://doi.org/10.1002/advs.202105076.
[53] H.T. Baytekin, A.Z. Patashinski, M. Branicki, B. Baytekin, S. Soh, B.A. Grazybowski, The mosaic of surface charge in contact electrification, Science 333 (2011) 308–312, https://doi.org/10.1126/science.1201512.
[54] V. Nguyen, R. Yang, Effect of humidity and pressure on the triboelectric nanogenerator, Nano Energy 2 (2013) 604–608, https://doi.org/10.1016/j.nanoen.2013.07.012.
[55] C. Xu, A.C. Wang, H. Zou, B. Zhang, C. Zhang, Y. Zi, L. Pan, P. Wang, P. Feng, Z. Lin, Z.L. Wang, Raising the working temperature of a triboelectric nanogenerator by quenching down electron thermionic emission in contact-electrification, Adv. Mater. 30 (2018) 201803968, https://doi.org/10.1002/adma.201803968.

Tianxiao Xiao received his M.Sc. degree from Beijing Institute of Nanoenergy and Nanosystems, Chinese Academy of Sciences. He is presently a PhD candidate at the Institute for Functional Materials, School of Natural Sciences, Technical University of Munich. His research interests are focused on energy harvesters and self-powered sensors, wearable electronics, IoT applications.

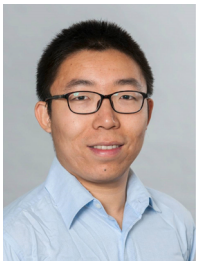

Dr. Zhenshan Bing received his doctorate degree in Computer Science from the Technical University of Munich, Germany, in 2019. He received his B.S degree in Mechanical Design Manufacturing and Automation from Harbin Institute of Technology, China, in 2013, and his M.Eng degree in Mechanical Engineering in 2015, at the same university. Dr. Bing is currently a postdoctroal researcher with Informatics 6, Technical University of Munich, Munich, Germany. His research investigates bioinspired robots which are controlled by artificial neural networks and related applications.

Yansong Wu received his M.Sc. degree in Electrical Engineering and Information Technology from Technical University of Munich, Germany, in 2022. He received his B.Sc. degree in Electrical Engineering and Automation from China Agricultural University, China, in 2018. Yansong Wu is currently a researcher with Munich Institute of Robotics and Machine Intelligence, Technical University of Munich, Munich, Germany.

Dr. Wei Chen is an Associate Professor with tenure in the College of Engineering Physics, at Shenzhen Technology University (SZTU), China. He obtained his Dr.rer.nat degree at the Technical University of Munich (TUM), Germany, in 2020. His research interests are focused on the correlations between the inner nanostructure and semiconductor performance of various solution-processed semiconductor thin films which involve colloidal quantum dots (CQDs), perovskites, and polymers. Particularly, his research team at SZTU is presently focusing on CQD-based short-wave infrared (SWIR) sensors.

Dr. Ziming Zhou received the Ph.D. degree from the National University of Singapore in 2022. He is currently an Assistant Research Fellow with the Institute of Advanced Displays and Imaging, Henan Academy of Sciences, Zhengzhou, China. His research focuses on ligand modification, alignment, and exploring the potential applications of semiconductor nanocrystals in the fields of displays and imaging.

Dr. Fan Fang received his Ph.D. in physical electronics from Southeast University in 2023 in China. He is currently a postdoctoral fellow at a joint program of Shenzhen Technology University and Shenzhen University. His research interests include the synthesis of quantum dots and the fabrication of quantum dots optoelectronic devices.

Suzhe Liang received his M.Sc. degree from North University of China with a joint-supervision program in Ningbo Institute of Materials Technology and Engineering, Chinese Academy of Sciences. He is presently a PhD candidate at the Institute for Functional Materials, Department of Physics, Technical University of Munich, Germany. His research interests involve anode materials for lithium/sodium-ion batteries and grazing incidence X-ray scattering techniques.

Dr. Renjun Guo is a research fellow in the Solar Energy Research Instituion at the National University of Singapore. He earned his PhD degree from the Department of Physics at the Technical University of Munich, Germany. He specializes in leveraging advanced characterization technologies, particularly synchrotron radiation light sources, to explore new frontiers in optoelectronic materials. His primary research thrust involves establishing correlations between morphological structures and the dynamics of charge carriers in optoelectronic materials. His scholarly contributions are reflected in numerous publications featured in globally recognized journals such as "Nature Energy", "Advanced Materials", and "Advanced Energy Materials".

Suo Tu is presently a Ph.D. student at the School of Natural Sciences, Technical University of Munich, under the supervision of Professor Peter Müller-Buschbaum. His current research is related to organic electronics and soft material systems.

Guangjiu Pan received his bachelor's degree from Jiangxi University of Science and Technology (2017) and his master's degree from Central South University (2020). Currently, he is a PhD candidate in Physics at Technical University of Munich, under the supervision of Prof. Dr. Peter Müller-Buschbaum since 2021. His research interests include the synthesis of mesoporous metal oxides based on block copolymer self-assembly and advanced X-ray scattering techniques.

Tianfu Guan is now a Ph.D. student at the Technical university of Munich, Germany. His research interests mainly focus on plasmonics, optoelectronic devices, and Granzing incidence X-Ray scattering(GIX).

Kai Wang, Ph.D., is currently a Professor of Southern University of Science and Technology (SUSTech). His research focuses on quantum dot optoelectronic devices and their applications in displays and photodetectors. He has published more than 200 articles on academic journals with h-index of 52 and an academic book. His research achievement is awarded the National Award for Technological Invention and the National Ministry of Education Award for Technological Innovation. He is the recipient of the National Outstanding Youth Scholar and also is selected as the World's Top 2% Scientists identified by Stanford University.

Dr. Xiao Wei Sun is a Chair Professor and the Executive Dean of the Institute of Nanoscience and Applications in the Southern University of Science and Technology (SUSTech). He is an Academician of the Asia-Pacific Academy of Materials. He is the fellow of several academic societies including Optica (formerly OSA), SPIE, SID and Institute of Physics (IoP, UK). His main research is on wide bandgap semiconductors and semiconductor nanocrystals for power-saving high-quality displays and lighting. Professor Sun has authored over 600 peer-reviewed journal publications, and delivered numerous invited talks. His H-index is 98. He is an Elsevier Highly Cited Scholar.

Dr. Kai Huang earned his Ph.D. degree at ETH Zurich, Switzerland, in 2010, his MSc from University of Leiden, the Netherlands, in 2005, and his BSc from Fudan University, China, in 1999. His research interests include techniques for the analysis, design, and optimization of embedded systems, particularly in the automotive and robotic domains. He was awarded the Program of Chinese Global Youth Experts 2014 and was granted the Chinese Government Award for Outstanding Self-Financed Students Abroad 2010. He has served as a member of the technical committee on Cybernetics for Cyber-Physical Systems of IEEE SMC Society since 2015.

Prof. Alois Knoll received his diploma (M.Sc.) degree in Electrical/Communications Engineering from the University of Stuttgart, Germany, in 1985 and his Ph.D. in Computer Science from Technical University of Berlin, Germany, in 1988. Since 2001, he has been a professor at the Department of Informatics, Technical University of Munich (TUM), Germany. His research interests include cognitive, medical and sensor-based robotics, multi-agent systems, data fusion, adaptive systems, multimedia information retrieval, model-driven development of embedded systems with applications to automotive software and electric transportation, as well as simulation systems for robotics and traffic.

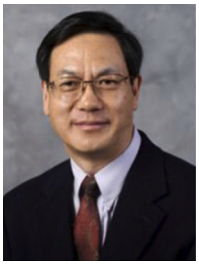

Prof. Zhong Lin (ZL) Wang received his Ph.D. from Arizona State University in physics. He is now the director of Beijing Institute of Nanoenergy and Nanosystems. Prof. Wang has made original and innovative contributions to the synthesis, discovery, characterization and understanding of fundamental physical properties of oxide nanobelts and nanowires, as well as applications of nanowires in energy sciences, electronics, optoelectronics and biological science. His discovery and breakthroughs in developing nanogenerators established the principle and technological road map for harvesting mechanical energy from environment and biological systems for powering personal electronics. His research on self-powered nanosystems has inspired the worldwide effort in academia and industry for studying energy for micro-nano-systems, which is now a distinct disciplinary in energy research and future sensor networks. He coined and pioneered the field of piezotronics and piezophototronics by introducing piezoelectric potential gated charge transport process in fabricating new electronic and optoelectronic devices. Details can be found at: www.nanoscience.gatech.edu.

Prof. Peter Müller-Buschbaum is full professor at Technical University of Munich, heading the Chair for Functional Materials since 2006. He is heading the Bavarian key laboratory 'TUM.solar' on solar energy conversion and storage and the 'Network for Renewable Energies'. He is the German representative at the 'European Polymer Federation' (EPF) for polymer physics. He is elected chairman of the 'Hamburg User Committee' (HUC) at the synchrotron radiation laboratory DESY, member of the 'European Synchrotron User Organization' (EUSO) and deputy editor of ACS Applied Materials & Interfaces. Since 2024, he is member of the TUM sustainability board. His research focuses on polymer nanohybrid materials with advanced scattering experiments.